Journal Name

ARTICLE TYPE

Cite this: DOI: 10.1039/xxxxxxxxxx

Ductile silica/methacrylate hybrids for bone regeneration

Anthony L. B. Maçon,[a] Siwei Li,[a] Justin J. Chung,[a] Amy Nommeots-Nomm,[a] Anu K. Solanki,[a] Molly M. Stevens,[a,b,c] and Julian R. Jones*[a]

Received Date
Accepted Date

DOI: 10.1039/xxxxxxxxxx

www.rsc.org/journalname

Bioglass® was the first synthetic material capable of bonding with bone without fibrous encapsulation, and fulfils some of the criteria of an ideal synthetic bone graft. However, it is brittle and toughness is required. Here, we investigated hybrids consisting of co-networks of high cross-linking density polymethacrylate and silica (class II hybrid) as a potential new generation of scaffold materials. Poly(3-(methoxysilyl)propyl methacrylate) (pTMSPMA) and tetraethyl orthosilicate (TEOS) were used as sol-gel precursors and hybrids were synthesised with different inorganic to organic ratios (I_h). The hybrids were nanoporous, with a modal pore diameter of 1 nm. At I_h = 50 %, the release of silica was controlled by varying the molecular weight of pTMSPMA while retaining a specific surface area above 100 m^2 g^{-1}. Strain to failure increased to 14.2 %, for I_h = 50 % using a polymer of 30 kDa, compared to 4.5 % for pure glass. The modulus of toughness (U_T) increased from 0.73 (pure glass) to 2.64 GPa. Although, the hybrid synthesised in this report did not contain calcium, pTMSPMA/SiO_2 hybrid was found to nucleate bone-like mineral on its surface after 1 week of immersion in simulated body fluid (SBF), whereas pure silica sol-gel glass did not. This increase in apatite forming ability was due to the ion-dipole complexation of calcium with the ester moieties of the polymer that were exposed after release of soluble silica from TEOS. No adverse cytotoxicity for MC3T3-E1 osteoblast-like cells was detected and improved cell attachment was observed, compared to a pure silica gel. pTMSPMA/SiO_2 hybrids have potential for the regeneration of hard tissue as they overcome the major drawbacks of pure inorganic substrates while retaining cell attachment.

Bone is the second most transplanted tissue after blood and musculoskeletal pathology treatments represent £10 billion per year in the U.K. alone.[1,2] Effective alternatives must be found to the current methods of skeletal defect treatments to avoid post-operation infection or revision, which can cost up to £70,000 per patient.[3] One attractive approach is to design biodegradable implants that could actively promote the bone growth and tissue remodelling by stimulating cellular activities whilst providing a mechanical support to the tissue.[4]

Bioglass® (BG), a biodegradable bioactive silicate glass (46.1 mol % SiO_2, 26.9 mol % CaO, 24.2 mol % Na_2O, 2.6 mol % P_2O_5), was the first material capable of bonding with bone by the formation of an apatite layer that forms on its surface after grafting.[5] A second mode of action is its dissolution products (in particular silica), which enhance osteoblast activities, whilst promoting extracellular matrix (ECM) production and cells differentiation.[6–8] 3D scaffolds have been produced from bioactive glasses, with interconnected pore networks in the form of foams[9,10] or 3-D printed structures[11], which can take load in compression, up to 150 MPa when 3D printed.[12] However, glasses are brittle and are unable to take cyclic loads. Biomaterials are needed that can share cyclic load with the host tissue, ideally matching its mechanical properties.

One strategy to overcome this shortfall in mechanical properties is to synthesise bioactive sol-gel silicate hybrids.[13–16] Sol-gel hybrids have nanoscale interpenetrated co-networks of inorganic and organic components. In class II hybrids the organic chains, usually polymers, covalently bond to the silica network.[14] Thus, polymers containing pendant alkoxysilane, -Si-$(OR)_3$ groups (R usually = methoxy or ethoxy), can hydrolyse, creating Si-OH groups, which can then undergo polycondensation with a conventional silica sol (from hydrolysed TEOS), forming Si-O-Si bonds, bridging the two networks.[17–19] Hybrids can therefore potentially benefit from the release of soluble silica whilst maintaining suitable mechanical properties due to the molecular rein-

* Corresponding author, E-mail: julian.r.jones@imperial.ac.uk
[a] Department of Materials Imperial College London, SW7 2AZ, London, UK. E-mail: julian.r.jones@imperial.ac.uk
[b] Institute of Biomedical Engineering Imperial College London, SW7 2AZ, London, UK.
[c] Department of Bioengineering Imperial College London, SW7 2AZ, London, UK.

forcement provided by the polymer. Additionally, and as opposed to a conventional composite, this strategy can allow congruent degradation of the inorganic and organic matrices.[20–22] Natural polymers, such as polypeptide, polysaccharide, or synthetic aliphatic polyesters have been used as organic components of hybrids. They require functionalisation with organosilicate coupling agents, such as 3-glycidoxypropyl trimethoxysilane (GPTMS), in order to form covalent bonds with the silica network.[20–22] However, the *in situ* reaction of GPTMS with polymers within the sol does not go to completion, forming by-products that are difficult to remove.[21,23] Methacrylate based polymers present several benefits for the synthesis of silica class II sol-gel hybrids as they can be designed with a variety of chemical groups, including alkoxysilane moieties that provide coupling sites for the silica network, structures and morphologies.[24] In addition, the cross-linking density (ability of a polymer molecule to covalently bond the silica network) can be controlled independently of the molecular mass of the polymer.

Previous work on silica class II hybrids based on polymethacrylate, for bone regeneration, featured random co-polymers synthesised with 3-(trimethoxysilyl)propyl methacrylate (TMSPMA) and methyl methacrylate (MMA) or 2-hydroxyethylmethacrylate (HEMA)[25–34]. In these reports, the cross-linking density (molar percentage of TMSPMA in the polymer) did not exceed 20 % and hybrids contained calcium salts as a promoter of bioactivity. Promising data was acquired, with nucleation of calcium phosphate on the surface of the hybrids in SBF, achieved within 24 h for poly(TMSPMA$_{10}$-*r*-HEMA$_{90}$)/$CaCl_2$, and the bulk Young's modulus reached 4±0.2 GPa for poly(TMSPMA$_{20}$-*r*-MMA$_{80}$)/SiO_2-$Ca(NO_3)_2$.[26,27,35] However, a significant scatter in properties was observed for hybrids with similar nominal compositions. For instance, Ravarian *et al.* reported three orders of magnitude lower Young's modulus for hybrids made with poly(TMSPMA-*r*-MMA) with consistent inorganic to organic weight ratio compared to Lee *et al.*. Many of the reports are missing polymer characterisation (molecular weight and structure). Thus, the scatter in properties may originate from significant variations in the polymer chemistry, which might affect its interaction and interpenetration with the silica matrix.

Here, we developed a comprehensive approach where a high cross-linking density polymer, homopolymer of TMSPMA, was used as an organic source for silicate class II hybrids to investigate structure-property relationships. The aim was to determine the effect of the molecular weight (MW) of the polymer on the mesoporosity and silica release rate in buffered media, to select an optimal composition in terms of delivery of soluble silica. pTMSPMA/SiO_2 hybrids were tested *via* compression test, calcium-phosphate nucleation ability and cell viability in compliance with the ISO 10993-5 and ISO 10993-12 standards. In the long term we expect the hybrid to undergo slow dissolution, losing soluble silica, then polymer molecules. Poly(TMSPMA) was designed to ensure it can pass through the kidneys and be excreted after dissolution.

1 Materials and experimental methods

1.1 Materials

All reagents were purchased from Sigma-Aldrich UK and used without further purification unless stated. 3-(Methoxysilyl)propyl methacrylate) (TMSPMA) was purified by distillation under reduce pressure. 2,2'-Azobisisobutylonitrile (AIBN) was recrystallised in cold methanol before use. Tetrahydrofuran (THF) was dried using 3 Å molecular sieves prior to any polymer synthesis.

1.2 Synthesis method

1.2.1 Polymer synthesis

Poly(3-(methoxysilyl)propyl methacrylate) (pTMSPMA) and its class II hybrids were synthesised following experimental procedures detailed elsewhere.[17] pTMSPMA was synthesised by regulated-free radical polymerisation using AIBN as initiator and thioglycerol as a chain transfer agent. The polymerisation was conducted in THF under argon for 24 h at 60°C. Subsequently, pTMSPMA was purified by precipitation in n-hexane, 3 times, dried in a vacuum desiccator for 2 h and redispersed in ethanol, $R_{EtOH} = \frac{n_{EtOH}}{n_{TMSPMA}} = 6$.

1.2.2 Hybrid synthesis

pTMSPMA/SiO_2 hybrids were synthesised using the sol-gel process with tetraethyl orthosilicate (TEOS) and pTMSPMA as precursors using acidic catalysis at room temperature. The mass of TEOS hydrolysed was calculated based on the mass of the polymer ($m_{polymer}$) and the intended inorganic to organic mass ratio (I_h), using Eq 1:

$$I_h = \frac{m_{SiO_2} + m_{SiO_{1.5}}}{mSiO_2 + m_{SiO_{1.5}} + m_{Org}} \Leftrightarrow$$

$$m_{TEOS} = \left(\frac{I_h}{1-I_h} * \frac{m_{polymer}}{M_{w,TMSPMA}} * M_{w,Org} - \frac{m_{polymer}}{M_{w,TMSPMA}} * M_{w,SiO_{1.5}}\right) * \frac{M_{w,TEOS}}{M_{w,SiO_2}} \quad (1)$$

The backbone of the polymer was considered as part of the organic component of the class II hybrid. Hydrochloric acid (HCl) and water were added relative to the number of alkoxy silane groups in TEOS and pTMSPMA according to the following ratios : $R_{HCl} = \frac{n_{HCl}}{n_{SiOR}} = 0.01$ and $R_{H_2O} = \frac{n_{H_2O}}{n_{SiOR}} = 1$. Water from HCl was subtracted according to the final amount of distilled water added. The solution was stirred at 1000 r.p.m, for 30 min, allowing TEOS to be hydrolysed, after which the purified polymer was added into the beaker. The mixture was allowed to mix for 30 s and cast into poly(tetrafluoroethylene) (PTFE) moulds and subsequently sealed. After 3 d of ageing, the lids were loosened for the solvent to evaporate. Si-pTMSPMA monoliths were considered to be dried when their mass stabilised.

1.2.3 Bioglass synthesis

Bioglass® (BG) (46.1 % SiO_2, 26.9 % CaO, 24.4 % Na_2O, 2.6 % P_2O_5, in mol.%) was synthesised by mixing the relevant oxides together and heating to 1420°C, in a platinum crucible, for 1.5 h followed by quenching in water at room temperature. The coarse frit form of the glass was collected and dried overnight. The solid

form of the glass was ground to a powder and sieved at <100 μm.

1.3 Characterisation

1.3.0.1 Nuclear magnetic resonance: The structure of pTMSPMA was assessed by ^{1}H NMR. Spectra were recorded in $CDCl_3$ using a Bruker AV-400 spectrometer operating at 400 MHz.

1.3.0.2 Size exclusion chromatography: Molecular weights were determined by size exclusion chromatography using Viscotek TDA 305 instrument (Malvern instrument, USA) equipped with Viscotek D6000M and D2500M columns. Linear poly(methyl methacrylate) was used as a standard for universal calibration. Dimethylformamide (DMF) with 0.075 % of lithium bromide was used as a mobile phase flowing at 0.7 mL min^{-1}, 35°C.

1.3.0.3 Specific surface area: Nitrogen sorption was used to determine the surface area of the hybrid (Autosorb AS1, QuantaChrome). Samples were degassed at 150°C for 8 h before analysis (Degasser, Quantachrome). Specific surface areas were calculated using the BET equation applied to the first 11 points on the adsorption branch of the isotherm, giving an R^2 >0.999.[36]

1.3.0.4 Compression tests: Uni-axial compression tests were performed on cylindrical shaped monoliths (diameter = 10 mm, height = 10 mm) following the British standard EN 658-2:2002.[37] Tests were performed on a Zwick 1474 fitted with a 100 kN load cell at a constant strain rate, 10 mm min^{-1}, until failure. The Young's Modulus, maximum compressive strength and strain to failure were determined from 5 repeats. The modulus of toughness was calculated by integrating the stress-strain curves using the built-in *integration* function of Matlab R2013b.[38]

1.3.0.5 Dissolution test: pTMSPMA/SiO_2 hybrids were immersed in media simulated body fluid (SBF) or 5 mM TRIS-HCl buffered water using a ratio of 75 mg glass to 50 mL of media in an airtight polyethylene container.[35] Dissolution vessels were placed in an incubating orbital shaker held at 37°C, agitated at 120 r.p.m. The pH (7.4) and temperature of the media were verified before use. The samples were incubated for 4 h, 8 h, 24 h, 72 h, 1 wk and 2 wk. At the end of each time period, the samples were removed from the incubator and the solids were collected by filtration (particle retention 5-13 μm). The powder was immediately washed with DI water and subsequently with acetone to terminate any reaction. Each sample was run in triplicate. The filtered solution was collected to determine the ion concentrations using an inductively coupled plasma (ICP) analysis; the pH of the solution was also measured. The same protocol was applied to the media alone as a control. Elemental concentrations in solution were measured with a Thermo Scientific iCAP 6300 Duo inductively coupled plasma-optical emission spectrometer (ICP-OES) with auto sampler. Sample solutions were prepared by diluting the samples by a factor of 10 with analytical grade 2 M HNO_3. Mixed standards of silicon, phosphorus, calcium, sodium and potassium were prepared at 0, 2, 5, 20 and 40 μg mL^{-1} for the calibration curve. Silicon and phosphorus were measured in the axial direction of the plasma flame whereas calcium, sodium and potassium were measured in the radial direction.

1.3.0.6 Fourier transform infrared spectroscopy: ATR-FTIR was performed on the purified polymers and the pTMSPMA/SiO_2 hybrids, before and after immersion in SBF, using a Nicolet iS10 fitted with a Specac MK11 Golden gate single reflection ATR module.

1.3.0.7 X-ray powder diffraction: X-ray diffraction (XRD) patterns were recorded before and after immersion in SBF using a Panalytical X'pert Pro MPD. The radiation source was a Ni filtered Cuκ_α. Diffraction was measured continuously from 6 to 70° 2θ, with a step size of 0.026° and a time per step of 100 s.

1.3.0.8 Scanning electron microscopy: Field emission gun scanning electron microscopy (FEG-SEM) was performed on a Leo 1525 with Gemini column fitted using a gun voltage of 5 kV for secondary electron imaging with a working distance of 6-13 mm. Samples were prepared by mounting them on double sided carbon tape and coating with chromium.

1.3.0.9 Zeta-potential and dynamic light scattering: The Malvern Zetasizer (instrument 2000) was used to measure the zeta potential and the hydrodynamic radius of the hybrids and polymers, respectively. Zeta potential measurement of the hybrids were carried out in PBS, 7.4 pH. Hydrodynamic radius of pTMSPMA was recorded in THF.

1.3.0.10 Cell viability: MC3T3-E1 preosteoblast cell line (ATCC, UK) was expanded in monolayer cultures in basal α-MEM supplemented with 10 % (v/v) FCS (foetal calf serum), 100 unit mL^{-1} penicillin and 100 μg mL^{-1} streptomycin. Cultures were maintained in humidified atmosphere at 37°C, 5 % CO_2 and 21 % O_2. Cells were passaged upon confluence using 500 μg mL^{-1} trypsin-EDTA (ethylene diamine tetra-acetic acid). Potential *in vitro* cytotoxicity effects of pTMSPMA/SiO_2 and pure silica gel (I100) on MC3T3-E1 cells were assessed in accordance to ISO 10993-5 and ISO 10993-12.[39,40] Dissolution products released by the samples (0.2 g mL^{-1} in α-MEM at 37°C) over a 72 h period were prepared. Medical grade polyethylene (PE) was used as negative control (non-cytotoxic) and poly urethane (PU) containing 0.1 % (w/w) zinc diethyldithiocarbamate (ZDEC) was used as positive control (provides reproducible cytotoxic response). The dissolution products were filter sterilised and, dilution series (25 %, 50 %, 75 % and 100 %) were prepared and supplemented with 10 % (v/v) FCS prior to use in cell viability assays. Cell viability was assessed by a calorimetric cell metabolic activity assay based on the conversion of 3-(4,5-dimethylthiazol-2-yl)-2,5-diphenyl tetrazolium bromide (MTT) into formazan. The optical density was measured spectrophotometrically at 570 nm using a microplate reader (SpectraMax M5). For cell attachment studies, pTMSPMA/SIO_2 and I100 disks (approximately 5x5x1 mm^3) were sterilised with 70 % ethanol for 1 min. Following washing with PBS, each sample was placed in serum-free α-MEM for 30 min prior to cell seeding. Monolayer expanded MC3T3-E1 cells were harvested and suspended in basal α-MEM at a concentration 1.10^5 cells mL^{-1}. 10 μL of cell suspension was seeded onto each pTMSPMA/SiO_2 and I100 disk and, incubated in humidified atmosphere at 37°C, 5 % CO_2 and 21 % O_2 for 2 h. Each cell-seeded disk was then submerged in fresh basal α-MEM and cultured for

further 24 h. Cell-seeded disks were fixed with 4 % paraformaldehyde (PFA) and used for immunohistochemical analysis of cell attachment. Following permeabilisation with buffered 0.5 % Triton X-100 in PBS (300 mM sucrose, 50 mM NaCl, 3 mM $MgCl_2$, 20 mM Hepes and pH 7.2) and blocking with 10 mg mL^{-1} BSA in PBS, samples were incubated with antybodies at 4°C for 1 h. Negative controls (omission of the primary antisera) were performed in all immunohistochemistry procedures. F-actin was labelled using CytoPainter F-actin staining kit (Abcam, Cambridge, UK) following the manufacture's instruction. Briefly, Alexa Fluor 568-conjugated phalloidin (1:1000 dilution in labelling buffer) was added simultaneously with the secondary antibody during the incubation period. All samples were counter-stained with DAPI (0.1 μg mL^{-1} in PBS), staining DNA. The samples were imaged under confocal microscopy (Leica SP5 MP laser scanning confocal microscope and software, Leica Microsystems, Wetzlar, Germany). Cells were also imaged by SEM after dehydratation using hexamethyldisilazane (HMDS).

2 Results and Discussion

2.1 Polymers and hybrids synthesis

Poly(3-(methoxysilyl)propyl methacrylate) (pTMSPMA) was synthesised via regulated-free radical polymerisation, targeting average molecular weights (M_n) of 2.5, 7.5, 15 and 30 kDa, using thioglycerol as a chain transfer agent.[17,41,42] The M_n of pTMSPMA was tailored such that it could pass through the porous glomerulus of the kidney and avoid accumulation in the liver.[43] pTMSPMA was therefore synthesised with a cut off in M_n of 30 kDa to potentially have a hydrodynamic radius under the renal threshold of 5 nm.[44] These requirements were met, as shown by dynamic light scattering, with R_h = 5.05 nm for pTMSPMA at 30 kDa and lower radii for polymers with a smaller M_n (Figure 1-a). The structure of pTMSPMA was evaluated by ^{1}H NMR, which was conducted after purification (Figure 1-b). Figure 1-b shows that TMSPMA polymerised successfully without any signs of hydrolysis of its alkoxy-silane moiety, which would translate to a decrease of the relative integration of the methoxy groups ($\delta \approx 3.58$ ppm) to the first protons on the propyl chain ($\delta \approx 3.90$ ppm) after polymerisation.[45,46] After purification and redispersion in ethanol, pTMSPMA was added to a solution of hydrolysed tetraethyl orthosilicate (TEOS) at different concentrations to aim at inorganic to organic ratios of 29 % (only the polymer), 50 % and 75 %, later called I29, I50, I75 respectively (Schematic of the reaction in Figure 2-a). A control, I100, consisting of a pure silica gel, was also synthesised under the same experimental conditions (pH, water content, ethanol content).

2.2 Porosity and silica release: effect of the pTMSPMA molecular weight

Soluble silica has been shown to be important for bone regeneration, increasing significantly the expression of collagen type I, up-regulating the expression of growth factors responsible for vascularisation and inhibiting the osteoclast activity.[47–50] The dissolution of silicate based bioactive glasses also caused the up-regulation of seven families of genes in primary human osteoblasts, promoting bone growth.[7] The effect of the dissolution ions (soluble silica and calcium ions) was found to be dose dependent on foetal osteoblasts.[51] Thus, it is important to understand the influence that pTMSPMA has both on the structure of the hybrid and the release of soluble silica. In addition to structure, the release of silica sol-gel is driven by mesoporosity, which is the primary factor that determines the specific surface area (SSA)[52]. While gels and glasses made by acidic catalysed sol-gel processing have inherent mesoporosity[53], the majority of previous work on hybrid synthesis does not report mesoporosity. Figure 2-b shows the effect of the molecular weight of pTMSPMA on the SSA at different inorganic to organic ratios. At I75, the SSA was independent of pTMSPMA with values close to the pure silica gel, SSA_{I100} = 457 m^2 g^{-1}. However, at I50 a clear trend was observed with a decrease of the SSA as the molecular weight of pTMSPMA decreased, ranging from $SSA_{I50,2.5kDa}$ = 117 m^2 g^{-1} to $SSA_{I50,30kDa}$ = 450 m^2 g^{-1}. When the polymer was cross-linked without TEOS, the calculated surface areas were below the detec-

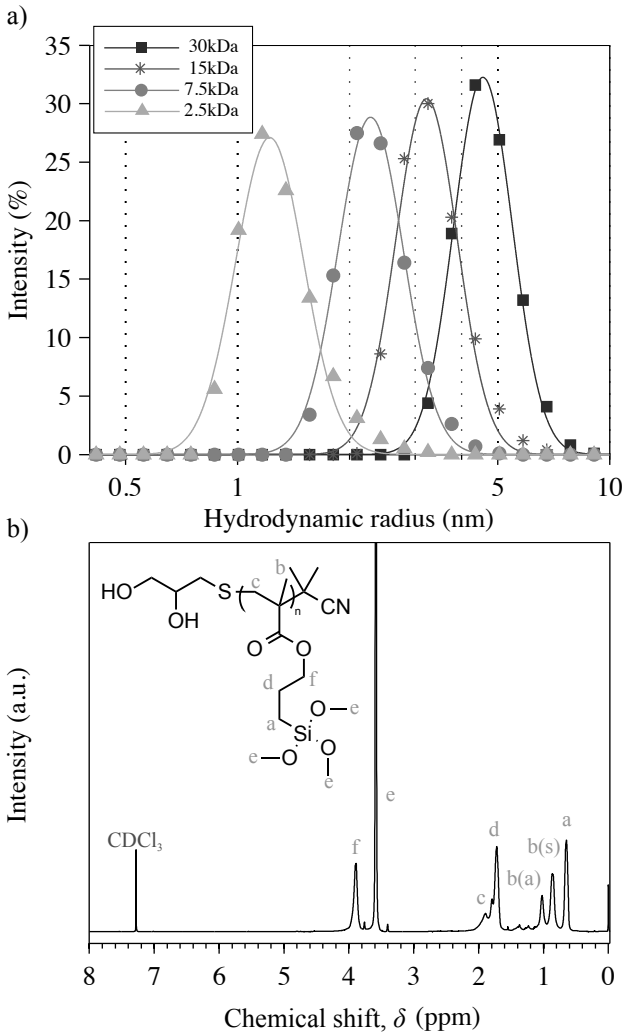

Fig. 1 a) Hydrodynamic radius of pTMSPMA at different M_n measured by dynamic light scattering in THF at 25°C b) ^{1}H NMR sprectrum of pTMSPMA in $CDCl_3$ after purification and its structural representation (inset).

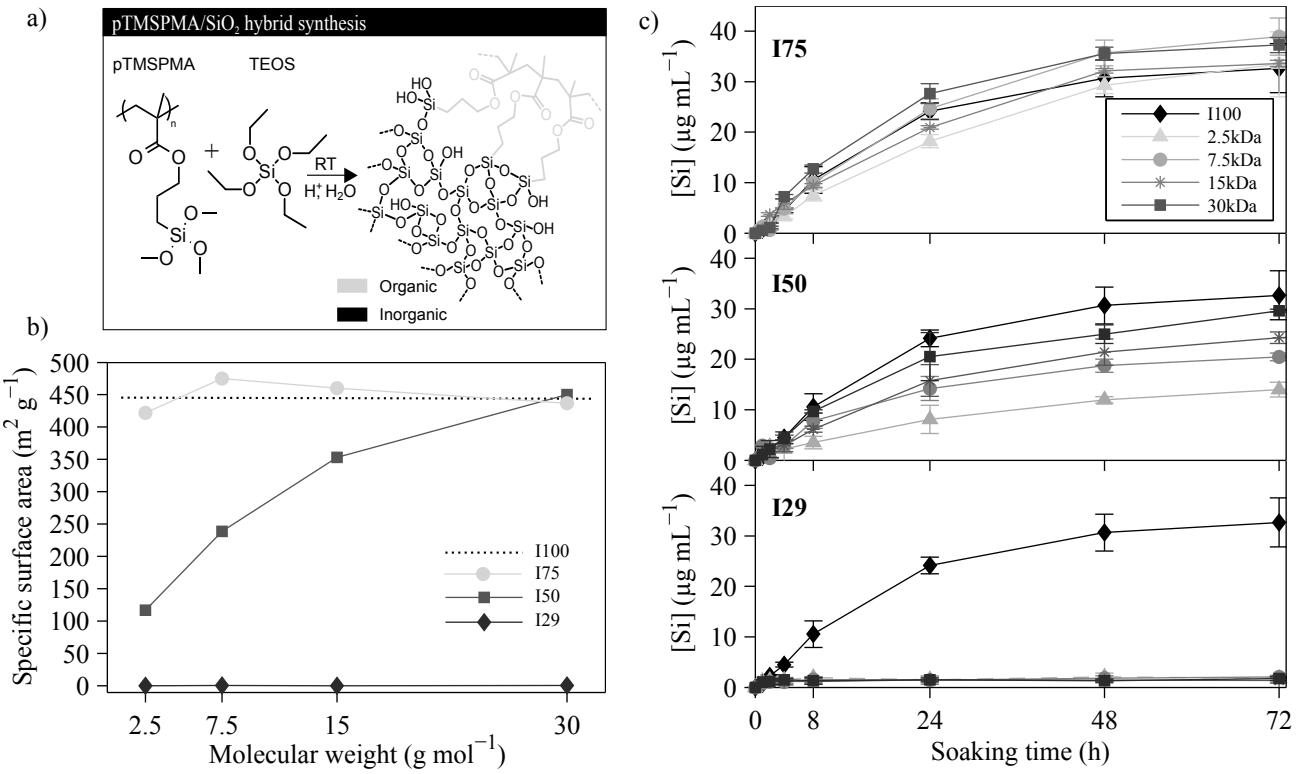

Fig. 2 a) Schematic of the hybrid synthesis; b) specific surface area of the hybrids as a function of pTMSPMA M_n and inorganic to organic ratio; c) silicon concentration profiles upon immersion of pTMSPMA/SiO_2 hybrid in aqueous 5 mM TRIS solution buffered at pH 7.35 over 3 d.

tion limit of 1 m^2 g^{-1}.[54,55] Thus, at I29 hybrids were not porous.

Variation in SSA was correlated with the release of soluble silica from the hybrids, which were immersed in a 5 mM TRIS aqueous solution at pH 7.35 over a period of 3 d as shown in Figure 2-c. For each inorganic to organic ratio, the silicon concentration profile of I100 was plotted as a control and showed an steady increase in the level of silica, reaching 39.1±3.9 μg mL^{-1} after 3 d. With hybrids at 75 % inorganic, the presence of pTMSPMA did not have any significant effect on the release of silica with trends and values statistically equivalent to the pure silica gel, I100. At I50, the same general observations on the trends were made with the concentration of silica increasing with time. However, the level of silica at 3 d varied depending on the M_n of pTMSPMA. As M_n increased the release of silica increased from 17.5±0.6 (2.5 kDa) up to 33.6±1.5 μg mL^{-1} (30 kDa). In addition, a linear relationship between the specific surface area and $[Si]_{I50,3d}$ was observed (R^2 = 0.97). At I29, hybrids did not show any sign of mesoporosity and only 1.73±0.35 μg mL^{-1} of silica was released in solution, which was close to the 1 μg mL^{-1} detection limit of the ICP-OES.

According to the analysis on the morphology of pTMSPMA/SiO_2 hybrids in our previous report, M_n of pTMSPMA influences the gelation mechanism.[17] At I50, the concentration of the pTMSPMA was higher than TEOS, and its hydrodynamic radius at least an order of magnitude larger than the dimers or cage-like structures that TEOS formed after 1 h of hydrolysis/condensation, which was the time at which the polymer was added. Hence, the gelation of the hybrid sol was due to the entanglement of pTMSPMA through its self-condensation, forming a polymer mesh in which TEOS condensed. The interspacing of these meshes was dependent on M_n of the polymer, the mesh size decreased as M_n decreased. Hence, the reduction in SSA and the level of silica released at 3 d (Figure 1-b,c) could be due to the decrease in size of the tetrasilica rich domains in the hybrids. In addition, the interconnectivity of these domains could decrease as M_n of pTMSPMA decreases. These hypotheses imply that only the silicate derived from the TEOS released soluble silica, as opposed to the silica in the TMSPMA.

2.3 Mechanical relevance of pTMSPMA/SiO_2 hybrid as an implant for bone regeneration

One of the challenges in designing scaffolds for bone regeneration is to bring adequate mechanical support during healing.[13] For example, the Young's modulus of a humerus, which has high content of cancellous bone, can range from 1.1 to 448 MPa and 0.03 to 6.3 MPa in compressive strength[56–58].

The reduced Young's modulus, previously determined by nanoindentation, of pTMSPMA/SiO_2 hybrids increased as a function of the inorganic to organic ratio from 1.41±0.23 GPa for I29 to 7.35±0.98 GPa for I75.[17] These values reflect the properties of bulk materials and are not representative of a functional implant which must be porous. Mahony *et al.*[20] showed that for silica-gelatin hybrids, the mechanical properties of open porous foams could be predicted by applying cellular solid theory.[59] As a result,

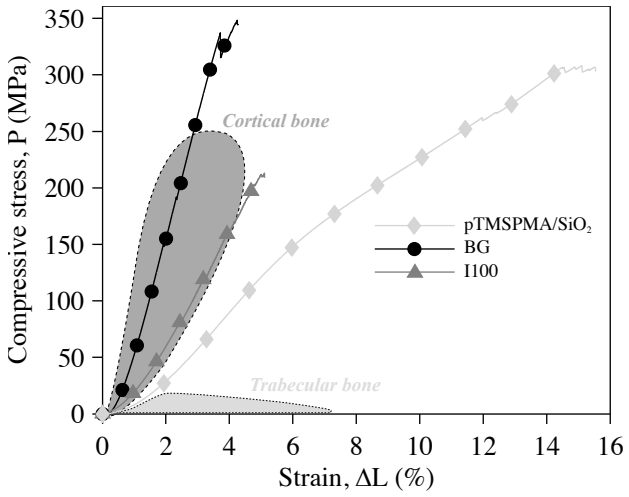

Fig. 3 Typical stress-strain curves obtained via uniaxial compression of BG, I100 and pTMSPMA/SiO_2 hybrid (I50, pTMSPMA at 30 kDa) at a strain rate of deformation of 10 mm min^{-1}. The pale grey and dark grey regions represents the range of mechanical properties of cortical and trabecular bone.

here, by targeting a porosity of 50 to 90 % similar to the apparent porosity of trabecular bone, hybrids made at an inorganic to organic ratio of 50 % would be mechanically suitable for defect repairs in non-load bearing bones, with Young's modulus ranging from 25.3 (90 % porosity) up to 632.5 MPa (50 % porosity), which is similar to cancellous bone.

Therefore, a pTMSPMA/SiO_2 hybrid with a inorganic to organic weight ratio of 50 % synthesised with pTMSPMA at 30 kDa was selected for its mechanical properties for further analysis.

2.3.1 Uniaxial compression:

Nanoindentation data, which have their limitations, give only the Young's modulus and the hardness. Further characterisation is needed to assess the ultimate strength. Thus, Young's modulus, modulus of toughness and ultimate strength of BG, I100 and pTMSPMA/SiO_2 were evaluated by uniaxial compression (Figure 3). Elastic deformation followed by brittle failure was observed for sol-gel derived I100 and melt derived BG. For both samples, small cracks along the direction of the load appeared and propagated when the compressive stress exceeded 100 MPa, leading to brittle failure at low strain of 4.5±1.2 % (Table 1). BG had a higher compression modulus than I100 with E=10.56±2.30 and E=7.97±1.59 GPa respectively. The mechanical properties of sol-gel silica glasses are directly influenced by the thermal stabilisation parameters and porosity.[63] Here, I100 was only dried up to 60°C, resulting in mesoporous silica gel monoliths. Consequently, I100 had lower mechanical properties than dense melt-derived BG. This is confirmed by the modulus of toughness, U_T, which is a measure of the energy absorbed by the material before complete failure (Table 1).[38] U_T for BG was 150 % larger (U_T = 0.73 GPa) than that of I100. Mechanical properties recorded for I100 and BG were in the same order of magnitude to that reported in the literature.[63,64]

pTMSPMA/SiO_2 had a different mode of deformation compared to BG and I100, with clear ductile behaviour. After elastic deformation, the yield strength was reached at 5.2 % of strain and 129.9±12.4 MPa of compressive stress, and was subsequently followed by plastic deformation with strengthening (strain hardening). Thus, pTMSPMA/SiO_2 had much higher toughness than its inorganic analogue, I100, with a modulus of toughness 550 % greater. It is likely that this ductility originated from the mobility of silica particles (from the condensation of TEOS) within the pTMSPMA mesh upon compression, allowing the hybrid to strain up to 14.2 % before fracture. pTMSPMA provided a molecular reinforcement to the silica matrix through covalent bonding. This substantial increase in toughness and strain to failure might be the key to increase the rather limited fatigue failure (limit of resistivity to cyclic-loading) characteristic of bioactive glasses and therefore avoid mechanical failure after grafting. However, the validation of this hypothesis is beyond the scope of this paper.

2.4 Evaluation of the *in vitro* performance of pTMSPMA/SiO_2 hybrid

In vitro experiments were conducted to determine whether pTMSPMA/SiO_2 hybrids have the potential to be used as bone implant: Apatite nucleation ability and measurement of osteoblast viability. These tests are not indicative of *in vivo* performance, yet can be used as reference for future design. The results obtained for hybrid were compared with I100 and BG.

2.4.1 Calcium-phosphate nucleation:

pTMSPMA/SiO_2 hybrid was immersed in simulated body fluid (SBF) over 2 wk to investigate its ability to nucleate a calcium phosphate layer.[35] This measurement is not to be related to the potential *in vivo* performance of the hybrid but to understand the change in chemistry (surface and ionic concentrations) upon immersion in media that have the same ionic strength that the body fluid present in a bone defect.[65] Variations in the concentration of silicon, calcium and phosphorus in SBF were monitored using ICP-OES along with the pH. Changes in surface chemistry were analysed by FTIR, XRD and SEM (Figure 4). Blank SBF, BG and I100 were incubated under the same conditions and used as a control. Upon immersion, the pH of SBF_{BG} increased from 7.45 to 8.17 due to the exchange of the cations (Ca^{2+} and Na^{+}) from the glass with the H_3O^{+} in solution whereas for I100 and hybrid, the pH remained within the buffering capacity of the media.[66] All solutions increased in silicon concentration following the same trend, reaching 50.4±0.4, 49.5±0.3 and 40.0±1.3 μg mL^{-1} for SBF_{BG}, SBF_{I100} and SBF_{Hybrid}, at 2 wks, respectively.

Depletion in calcium or phosphorus concentration is known to be a good indicator of calcium phosphate nucleation onto the surface of bioactive glasses.[35,67] Here, BG and I100 behaved as described in the literature with limited bioactivity observed for I100 and rapid variation in the ionic strength of SBF upon immersion of BG due to the nucleation of a calcium-phosphate layer on its surface.[68,69] Due to the similarity between I100 and the inorganic component of pTMSPMA/SiO_2, their apatite forming ability was expected to be at a similar rate. However, after 1 week of immersion, the level of calcium and phosphorus dropped signif-

Table 1 Summary of the mechanical properties of BG, I100 and I50, 30 kDa pTMSPMA/SiO_2 hybrid in uniaxial compression. The properties in compression of trabecular and cortical bones are given as a comparison.[60–62]

Entry	Young's modulus E (GPa)	Modulus of toughness, U_T (GPa)	Yield strength		Ultimate strength	
			Stress (MPa)	Strain (%)	Stress (MPa)	Strain (%)
Cortical bone	7-30	0.5-1.5	0.5-1	100-230	100-230	1-3
Trabecular bone	0.5-0.05	-	-	-	2-12	5-7
BG	10.56±2.30	0.73	-	-	345.8	4.2
I100	7.97±1.59	0.48	-	-	210.2	4.9
pTMSPMA/SiO_2	3.14±0.41	2.64	129.9	5.2	301.3	14.2

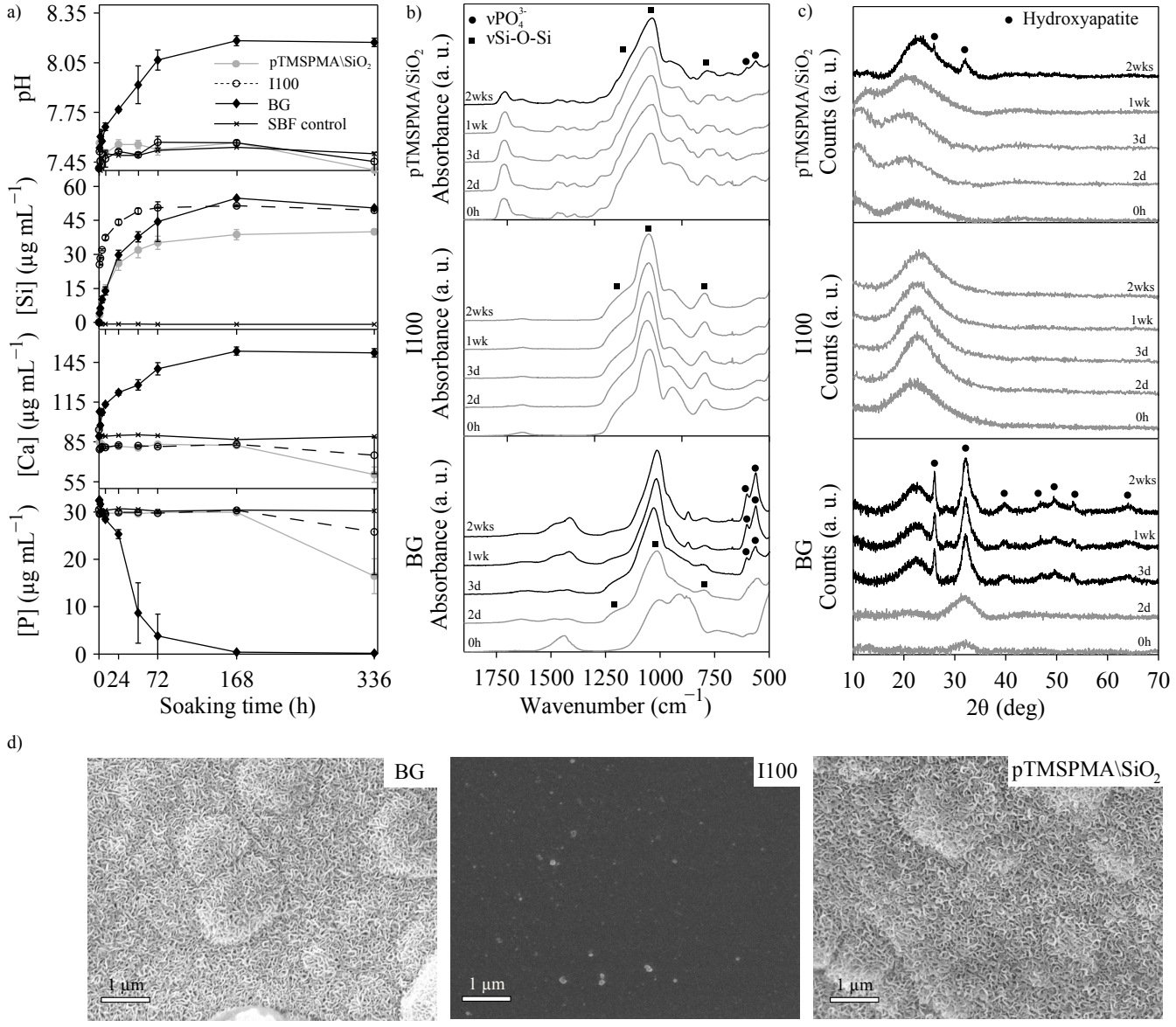

Fig. 4 a) pH and silicon, calcium and phosphorus concentration profiles upon immersion in SBF of BG, I100 and pTMSPMA/SiO_2 hybrid over 2 wk, b) and c) are the change in surface chemistry observed at different time points by FTIR and XRD, respectively. d) SEM images of surfaces of BG, I100 and pTMSPMA/SiO_2 hybrid (I50, pTMSPMA at 30 kDa) after 2 wks in SBF.

icantly for pTMSPMA/SiO_2 hybrid compared to the SBF control and I100, with concentration reaching 16.4±3.7 μg mL^{-1} for P and 60.4±5.8 μg mL^{-1} for Ca at 2 wks of immersion, suggesting that a calcium-phosphate layer was forming on the surface of the hybrid.

To ensure that the depletion in calcium and phosphorus level was not due to an instability of the SBF solution but to the nucleation of a calcium-phosphate (Ca-P) crystal onto the surface of the hybrid, FTIR, XRD and SEM were conducted on the collected powder after immersion (Figure 4). Before soaking in SBF,

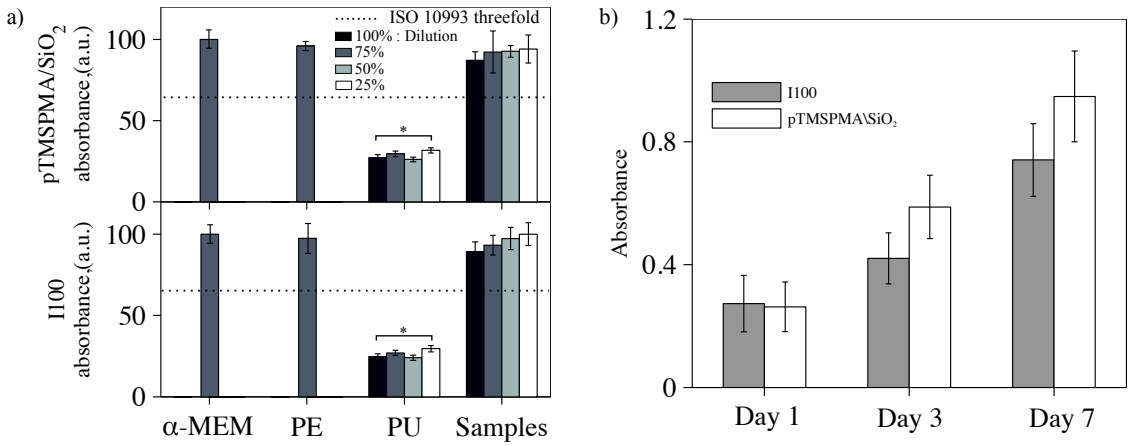

Fig. 5 a) Cell viability (MC3T3 cell line) test following the ISO 10993-5 and -12, every set of data is normalised to the optical density of the culture media; α-MEM = standard culture media, PE = polyethylene (-ve control), PU = polyurethane (+ve control), * indicates p<0.05, N=3 for all tests. Percentages given in PU and samples bars represents different dilution factors of the dissolution product with fresh culture media. b) MTT assay over 7 d of culture comparing the proliferation of pTMSPMA/SiO_2 hybrid (I50, pTMSPMA at 30 kDa) and I100.

Table 2 ζ-potential of I100 and pTMSPMA/SiO_2 hybrid (I50, pTMSPMA at 30 kDa) after immersion in 5 mM TRIS solution. Measurements were taken 5 min after dispersion in PBS (pH=7.4).

Incubation (days)	ζ_{I100} (mV)	ζ_{hybrid} (mV)
0	-17.2±2.4	-14.2±0.4
3	-15.3±4.3	-17.4±2.1
7	-16.3±1.2	-20.1±4.1
14	-14.8±0.8	-26.7± 1.1

all samples presented similar FTIR spectra with strong absorption bands at 1020 and 800 cm^{-1} due to their Si-O-Si silica network. XRD patterns were also similar with amorphous halos at $\theta \approx 32^\circ$ for BG and $\theta \approx 22^\circ$ for I100 and pTMSPMA/SiO_2 hybrid. BG induced nucleation and crystallisation of Ca-P within 3 d of immersion in SBF, due to the local increase in pH due to ion exchange of cations from the glass with protons from the SBF, and the abundance of Si-OH groups on it surface that acts as nucleation sites. Crystallisation of the Ca-P layer is associated with the FTIR detection of P-O bending bands at 565 and 605 cm^{-1} and stretching band at 1030 cm^{-1}, characteristic of the tetrahedral PO_4^{3-} groups in a crystal orthophosphate lattice, and sharp X-ray diffraction peaks at $\theta \approx 26^\circ$ and $\theta \approx 32^\circ$, confirming hydroxycarbonated apatite (HCA) formation (ICSD 01-084-1998). Similar features were detected on the surface of the hybrid after 2 wk, confirming that the drop in phosphorus and calcium levels was due the nucleation of HCA. Additionally, the hybrid and BG were fully covered by the characteristic HCA needle-like crystals as shown by SEM (Figure 4-d). However, the mechanism that led to the formation of this Ca-P layer differed to BG, as the hybrid did not contain any calcium and the pH remained approximately constant over the incubation period. The introduction of the polymer into the sol-gel process improved apatite forming ability over that of I100.

To get a better insight on the difference in apatite forming ability between I100 and hybrid, the effect of the silica release on the surface charge of I100 and pTMSPMA/SiO_2 was monitored by measuring the ζ-potential of the powder collected after immersion in 5 mM TRIS-HCl, redispersed in PBS (Table 2). The surface charge of I100 did not significantly vary upon immersion in buffered water, over the 2 wks of incubation, with a mean value of ζ_{I100}= -15.9±1.1 mV, as seen previously for sol-gel silica glass.[70,71] The pTMSPMA/SiO_2 hybrid behaved differently, with a steady decrease in ζ-potential from -14.2±0.4 mV to -26.7±1.1 mV over the 2 wks of incubation. The potential reached at 1 wk was comparable to poly(methyl methacrylate) measured under similar ionic strength and pH conditions, suggesting that, upon release of soluble silica from the condensed TEOS, a polymer rich layer was formed on the surface of the hybrid.[72,73] In addition, Zainuddin *et al.* demonstrated by ^{1}H NMR that in presence of Ca^{2+}, the ester groups of polymethacrylates can form a ion-dipole complex, inducing calcification.[74] This corroborates the drop observed in ζ-potential as the complexation of cations lowers the potential but also gives an insight on the mechanism Ca-P nucleation onto the surface of the hybrid, which is preferential on negatively charge surfaces. Moreover, Tanahashi and Matsuda showed that the polar affinity of cations for ester groups is a better inducer of apatite growth than silanol (Si-OH) moieties.[75] Thus we can hypothesise the following mechanism: upon immersion of pTMSPMA/SiO_2 hybrid in SBF, silica was released from its surface, generating a pTMSPMA rich layer, which induced complexation of Ca^{2+} through polar interactions with the ester groups from methacrylate, which induced the nucleation of a Ca-P layer.

2.4.2 Cell Viability:

The behaviour/fate of preosteoblast cells (MC3T3-E1) was assessed by exposition to the dissolution products of pTMSPMA/SiO_2 hybrid and I100 or when seeded directly onto the samples. Here, BG was not used as a control due to the large difference in composition with pTMSPMA/SiO_2 hybrid or I100. It is noteworthy to mention that the samples tested here were not pre-conditioned. Thus, an MTT assay was performed in accordance to ISO 10993-5 and 10993-12 to evaluate the cytotoxicity of the samples using their dissolution products. In ISO 10993 (Biological evaluation of medical devices), reduction

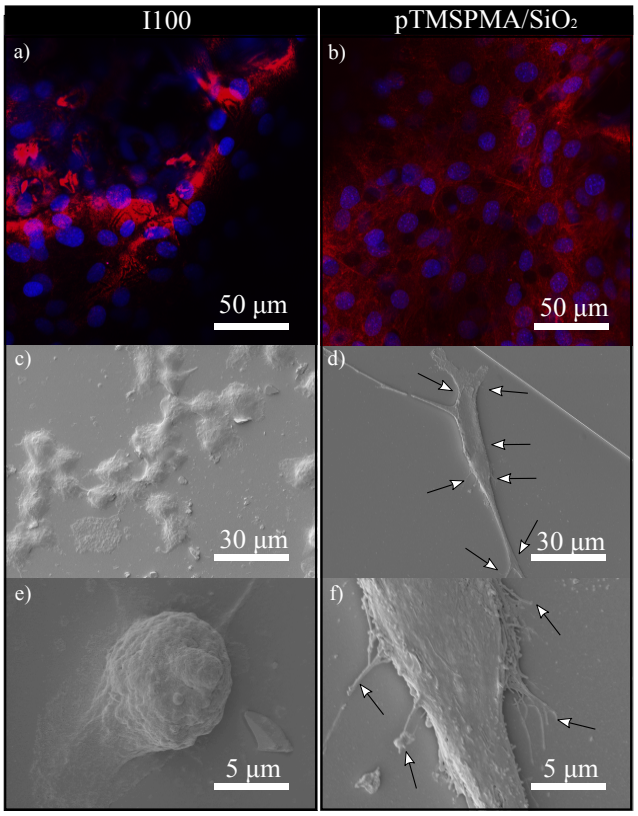

Fig. 6 a) b) Confocal images of I100 and pTMSPMA/SiO_2 hybrid (I50, pTMSPMA at 30 kDa) of MC3T3 cells 24 h after seeding where F-actin filament (red) were counter-stained with Alexa Fluor 568-conjugated phalloidin and DNA (blue) was counter stained with DAPI; c), d), e) and f) are SEM images of MC3T3 cells, 24 h after seeding. The arrows are pointing towards filopodia.

of cell viability exceeding more than 30 % in comparison to non-toxic controls is considered cytotoxic. The results confirmed that both I100 and pTMSPMA/SiO_2 did not induce any cytotoxic effects on MC3T3 cells *in vitro* (Figure 5-a). In addition, cells were capable of proliferation steadily over a period of 7 d in the presence of dissolution products of either pTMSPMA/SIO_2 or I100, obtained from 3 d incubation in α-MEM at 75 mg mL^{-1} (Figure 5-b). Cells cultured in pTMSPMA/SiO_2 dissolution products appeared to have a higher metabolic activity up to 7 d in comparison to those cultured in I100 dissolution products. However, the differences were not statistically significant.

Cell attachment on I100 and pTMSPMA/SiO_2 disks were examined by immunohistochemistry (IHC) and SEM (Figure 6). Following 24 h of culture, MC3T3 cells on pTMSPMA/SiO_2 disks demonstrated notably more robust expression of F-actin in comparison to those on I100 disks (Figure 5- A & B). The formation of higher order structures such as stress fibres was only visible in MC3T3 cells cultured on pTMSPMA/SiO_2 disks, suggesting established cell-cell and cell-ECM interactions.[76] In addition, SEM imaging confirmed the existence of filopodia only in MC3T3 cells cultured on pTMSPMA/SiO_2 disks (Figure 5-C & B). The formation of focal adhesions suggest that, in comparison to I100, pTMSPMA/SiO_2 is a superior material for promoting cellular attachment, which plays central role in tissue regeneration.[77] It is reported that cellular viability and survival is reduced if the extent of cell spreading area is very small (i.e. attachment of round cells without formation of focal contacts).[78] Limited spreading in MC3T3 cells cultured on I100 disks can be correlated to the reduced cellular metabolic activity observed in MTT assays. The size and shape of the spreading of cells on biomaterials, along with the number, shape and distribution of focal adhesions are dependent on a number of factors including surface charge, mechanical properties, wettability, surface roughness/topography, solubility, porosity, pH and the presence of functional groups.[79,80] Furthermore, different cell types react differently to biomaterials.[81–83] Therefore, it is difficult to draw a conclusive explanation for the different cell behaviour of MC3T3 cells when cultured on pTMSPMA/SiO_2 and I100 disks. The combination of a more hydrophilic, negatively charged surface and the inherent chemistry of pTMSPMA is likely to contribute to the improved cell attachment and spreading.

3 Conclusions

Here pTMSPMA/SiO_2 class II hybrids were successfully synthesised. The addition of a high cross linking density polymer into the sol-gel significantly improved the mechanical properties compared to sol-gel silica gel by changing the mode of deformation from brittle to ductile while retaining high specific area, mesoporosity and ability to deliver soluble silica. The presence of the polymer also improved the bone-like apatite forming ability compared to silica gel due to a decrease in the surface charge of the hybrid, which increased the rate of nucleation of bone like mineral on its surface. Improved cellular attachment was observed on the hybrid without apparent adverse cytotoxicity as compared to I100. Thus, pTMSPMA/SiO_2 hybrids have great potential for producing scaffolds with enhanced elasticity for bone regeneration while delivering soluble silica to the defect site and efficiently welcoming surrounding osteogenic cells.

4 Acknowledgement

The authors thank EPSRC (EP/I020861/1) for funding. Raw data can be obtained from julian.r.jones@imperial.ac.uk

References

1 T. Briggs, *A national review of adult elective orthopeadic services in the England*, B.o.a. technical report, 2015.
2 H. Shegarfi and O. Reikeras, *J. Orthop. Surg. Res.*, 2009, **17**, 206–11.
3 T. W. Briggs, *Improving the quality of orthopeadic care within the national health service in England*, B.o.a. technical report, 2012.
4 A. Oryan, S. Alidadi, A. Moshiri and N. Maffulli, *J. Orthop. Surg. Res.*, 2014, **9**, 1–27.
5 L. L. Hench, R. J. Splinter, W. C. Allen and T. K. Greenlee, *Journal of Biomedical Material Research*, 1971, **5**, 117–141.
6 I. D. Xynos, M. V. J. Hukkanen, J. J. Batten and L. D. Buttery, *Calcified Tissue International*, 2000, **67**, 321–329.
7 I. D. Xynos, A. J. Edgar, L. D. K. Buttery, L. L. Hench and J. M.

Polak, *J. Biomed. Mater. Res*, 2001, **55**, 151–157.
8 E. M. Carlisle, *Science*, 1972, **178**, 619–621.
9 J. R. Jones, L. M. Ehrenfield and L. L. Hench, *Biomaterials*, 2006, **27**, 964–973.
10 Z. Y. Wu, R. G. Hill, S. Yue, D. Nightingale, P. D. Lee and J. R. J. Jones, *Acta Biomater.*, 2011, **7**, 1807–1816.
11 X. Liu, M. N. Rahaman, G. E. Hilmas and B. S. Bal, *Acta Biomater.*, 2013, **9**, 7025–7034.
12 Q.Fu, E. Saiz and A. P. Tomsia, *Adv. Func. Mater.*, 2011, **21**, 1058–1063.
13 J. R. Jones, *Acta Biomaterialia*, 2013, **9**, 4457–4486.
14 B. M. Novak, *Adv. Mater.*, 1993, **5**, 422–432.
15 M.-Y. Koh, M. Kamitakahara, I. Y. Kim, K. Kikuta and C. Ohtsuki, *J. Mater. Sci. Mater. Med.*, 2010, **21**, 385–392.
16 M. M. Pereira, J. R. Jones, R. L. Orefice and L. L. Hench, *J. Mater. Sci. Mater. Med.*, 2005, **16**, 1045–1050.
17 A. L. B. Maçon, S. J. Page, J. J. Chung, N. Amdursky, M. M. Stevens, J. V. M. Weaver, J. V. Hanna and J. R. Jones, *Phys. Chem. Chem. Phys.*, 2015, **17**, 29124–29133.
18 A. L. B. Maçon, S. L. Greasley, C. R. Becer and J. R. Jones, *Macromol. Rapid Commun.*, 2015, **36**, 1806–1809.
19 J. J. Chung, T. K. Georgiou and J. R. Jones, *Macromol. Rapid Commun.*, 2015, **36**, 2060–2064.
20 O. Mahony, O. Tsigkou, C. Ionescu, C. Minelli, L. Ling, R. Hanly, M. E. Smith, M. M. Stevens and J. R. Jones, *Adv. Funct. Mater.*, 2010, **20**, 3835–3845.
21 L. S. Connell, F. Romer, M. Suárez, E. M. Valliant, Z. Zhang, P. D. Lee, M. E. Smith, J. V. Hanna and J. R. Jones, *J. Mater. Chem. B.*, 2014, **2**, 668.
22 G. Poologasundarampillai, B. Yu, O. Tsigkou, E. Valliant, P. D. Lee, R. W. Hamilton, M. M. Stevens, T. Kasuga and J. R. Jones, *Soft Matter*, 2012, **8**, 4822–4832.
23 L. Gabrielli, L. S. Connell, L. Russo, J. Jiménez-Barbero, F. Nicotra, L. Cipolla and J. R. Jones, *RSC Adv.*, 2014, **4**, 1841.
24 A. Gregory and M. H. Stenzel, *Prog. Polym. Sci.*, 2012, **37**, 38–105.
25 R. Ravarian, H. Wei, A. Rawal, J. Hook, W. Chrzanowski and F. Dehghani, *J. Mater. Chem. B*, 2013, **1**, 1835–1845.
26 R. Ravarian, X. Zhong, M. Barbeck, S. Ghanaati, C. J. Kirkpatrick, C. M. Murphy, A. Schindeler, W. Chrzanowski and F. Dehghani, *ACS Nano*, 2013, **7**, 8469–8483.
27 K.-H. Lee and S.-H. Rhee, *Biomaterials*, 2009, **30**, 3444–3449.
28 S.-H. Rhee, M.-H. Hwang, H.-J. Si and J.-Y. Choi, *Biomaterials*, 2003, **24**, 901–906.
29 S.-H. Rhee and J.-Y. Choi, *J. Am. Ceram. Soc.*, 2002, **85**, 1318–1320.
30 L. John, M. Baltrukiewicz, P. Sobota, R. Brykner, L. Cwynar-Zajac and P. Dziegiel, *Materials Science and Engineering C*, 2012, **32**, 1849–1858.
31 C. Ohtsuki, T. Miyazaki, M. kamitakahara and M. Tanihara, *Journal of the European Ceramic Society*, 2007, **27**, 1527–1533.
32 C. Ohtsuki, T. Miyazaki and M. Tanihara, *Materials Science and Engineering C*, 2002, **22**, 27–34.
33 T. Uchino, C. Ohtsuki, M. Kamitakahara, T. Miyazaki, S. Hayakawa and A. Osaka, *J. Biomater. Appl.*, 2008, **0**, 1–14.
34 T. Miyazaki, C. Ohtsuki and M. Tanihara, *J. Nanosci. Nanotechno.*, 2003, **3**, 511–515.
35 A. L. B. Maçon, T. B. Kim, E. M. Valliant, K. Goetschius, R. K. Brow, D. E. Day, A. Hoppe, A. R. Boccaccini, I. Y. Kim, C. Ohtsuki, T. Kokubo, A. Osaka, M. Vallet-Regí, D. Arcos, L. Fraile, A. J. Salinas, A. V. Teixeira, Y. Vueva, R. M. Almeida, M. Miola, C. Vitale-Brovarone, E. Verné, W. Höland and J. R. Jones, *J. Mater. Sci. Mater. Med.*, 2015, **26**, 115.
36 S. Brunauer, P. H. Emmett and E. Teller, *J. Am. Chem. Soc.*, 1938, **60**, 309–319.
37 *BS EN 658-2:2002 - Advanced technical ceramics - Mechanical properties of ceramic composites at room temperature-*.
38 L.-N. Niu, K. Jiao, Y.-P. Qi, C. K. Y. Yiu, H. Ryou, D. D. Arola, J.-H. Chen, L. Breschi, D. H. Pashley and F. R. Tay, *Angew. Chem. Int. Ed.*, 2011, **50**, 11688–11691.
39 *ISO 10993-12:2012 - Biological evaluation of medical devices – Part 12: Sample preparation and reference materials*.
40 *ISO 10993-5:2009 - Évaluation biologique des dispositifs médicaux – Partie 5: Essais concernant la cytotoxicité in vitro*.
41 J. V. M. Weaver, R. T. Williams, B. J. L. Royles, P. H. Findlay, A. I. Cooper and S. P. Armes, *Soft Matter*, 2008, **4**, 985–992.
42 F. Pardal, V. Lapinte and J.-J. Robin, *Eur. Polym. J.*, 2009, **45**, 1198–1207.
43 M. E. Fox, F. C. Szoka and J. M. J. Fréchet, *Accounts of Chemical Research*, 2009, **42**, 1141–1151.
44 T. Arai, N. Sawatari, T. Yoshizaki, Y. Einaga and H. Yamakawa, *Macromolecules*, 1996, **29**, 2309–2314.
45 J. Du and Y. Chen, *Macromolecules*, 2004, **37**, 6322–6328.
46 V. Mellon, D. Rinaldi, E. Bourgeat-Lami and F. D'agosto, *Macromolecules*, 2005, **38**, 1591–1598.
47 J. R. Henstock, L. T. Canham and S. I. Anderson, *Acta Biomater.*, 2015, **11**, 17–26.
48 Ž. Mladenović, A. Johansson, B. Willman, K. Shahabi, E. Björn and M. Ransjö, *Acta Biomater.*, 2014, **10**, 406–418.
49 H. Li and J. Chang, *Acta Biomater.*, 2013, **9**, 6981–6991.
50 D. M. Reffitt, N. Ogston, R. Jugdaohsingh, H. F. J. Cheung, B. A. J. Evans, R. P. H. Thompson, J. J. Powell and G. N. Hampson, *Bone*, 2003, **32**, 127–135.
51 O. Tsigkou, J. R. Jones, J. M. Polak and M. M. Stevens, *Biomaterials*, 2009, **30**, 3542–3550.
52 E. M. Valliant, C. A. Turdean-Ionescu, J. V. Hanna, M. E. Smith and J. R. Jones, *J. Mater. Chem.*, 2012, **22**, 1613–1619.
53 S. Lin, C. Ionescu, K. J. Pike, M. E. Smith and J. R. Jones, *J. Mater. Chem.*, 2009, **19**, 1276–1282.
54 K. S. W. Sing, D. H. Everett, R. A. W. Haul, L. Moscou, R. A. Pierotti, J. Rouquerol and T. Siemieniewska, *Pure & appl. Chem.*, 1985, **57**, 603–619.
55 S. Lowell, J. E. Shields, M. A. Thomas and M. Thommes, *Characterization of porous solids and powders: surface area, pore size and density (particle technology series)*, Springer Netherlands, 2004.
56 S. A. Goldstein, *J. Biomechanics*, 1987, **20**, 1055–1061.

57 L. J. Gibson, *J. Biomechanics*, 1985, **18**, 317–328.

58 J.-Y. Rho, L. Kuhn-Spearing and P. Zioupos, *Medical Engineeringh and Physics*, 1998, **20**, 92–102.

59 L. J. Gibson and M. F. Ashby, *Cellular solids: structure and properties*, Cambridge University Press, 1999.

60 L. L. Hench, *Biomaterial, artificial organs and tissue engineering*, Woodhead Publishing, 2005.

61 D. T. Reilly, A. H. Burstein and V. H. Frankel, *J. Biomechanics*, 1974, **7**, 271–275.

62 C. Mercer, M. Y. He, R. Wang and A. G. Evans, *Acta Biomater.*, 2006, **2**, 59–68.

63 T. Adachi and S. Sakka, *J. Mater. Sci.*, 1990, **25**, 4723–4737.

64 L. L. Hench, *J. Am. Ceram. Soc.*, 1998, **81**, 1705–28.

65 M. Bohner and J. Lemaitre, *Biomaterials*, 2009, **30**, 2175–2179.

66 M. Cerruti, D. Greenspan and K. Powers, *Biomaterials*, 2005, **26**, 1665–1674.

67 J. R. Jones, P. Sepulveda and L. L. Hench, *J. Biomed. Mater. Res.*, 2001, **58**, 720–726.

68 P. Saravanaparan and L. L. Hench, *J. Biomed. Mater. Res*, 2001, **54**, 608–618.

69 P. Sepulveda, J. R. Jones and L. L. Hench, *J. Biomed. Mater. Res*, 2002, **61**, 301–311.

70 S. Lin, W. V. den Bergh, S. Baker and J. R. Jones, *Acta Biomater.*, 2011, **7**, 3606–3615.

71 J. Coreno, A. Martínez, A. Bolarín and F. Sánchez, *J. Biomed. Mater. Res.*, 2001, **57**, 119–125.

72 H. Falahati, L. Wong, L. Davarpanah, A. Garg, P. Schmitz and D. P. J. Barz, *Electrophoresis*, 2014, **35**, 870–882.

73 B. J. Kirby and E. F. H. Jr., *Electrophoresis*, 2004, **25**, 203–213.

74 Zainuddin, D. J. T. Hill, A. K. Whittaker, L. Lambert and T. V. Chirila, *J. Mater. Sci. Mater. Med.*, 2007, **18**, 1141–1149.

75 M. Tanahashi and T. Matsuda, *J. Biomed. Mater. Res.*, 1997, **34**, 305–315.

76 A. Shamloo, *Cytoskeleton (Hobeken)*, 2014, **71**, 501–12.

77 C. M. Franz, G. E. Jones and A. J. Ridley, *Dev. Cell.*, 2002, **2**, 153–8.

78 M. A. Schwartz and R. K. Assoian, *J. Cell. Sci.*, 2001, **114**, 2553–60.

79 P. Slepicka, N. S. Kalsalkova, J. Siegel, Z. Kolska, L. Bacakova and V. Svorcik, *Biotechnol. Adv.*, 2015.

80 L. Bacakova, E. Filova, F. Rypacek, V. Svorcik and V. Stary, *Physiol. Res.*, 2004, **53**, S35–45.

81 A. J. Engler, S. Sen, H. L. Sweeney and D. E. Discher, *Cell*, 2006, **126**, 677–89.

82 N. Wang, K. Naruse, D. Stamenovic, J. J. Fredberg, S. M. Mijailovich and I. M. Tolic-Norrelykke, *Proc. Natl. Acad. Sci, USA*, 2001, **98**, 7765–70.

83 M. G. Marquez, Y. R. Brandan, V. E. Guaytima, C. H. Pavan, N. O. Favale and N. B. Speziale, *Biochym. Biophys. Acta.*, 2014, **1843**, 2991–3003.